J Mater Sci (2016) 51:2141–2152
DOI 10.1007/s10853-015-9524-9

Modeling of eutectic dendrite growth in undercooled binary alloys

Wangwang Kuang[1] · Haifeng Wang[1] · Feng Liu[1] · S. L. Sobolev[2]

Received: 12 August 2015 / Accepted: 20 October 2015 / Published online: 28 October 2015

Abstract A eutectic dendrite growth model in which the interface, solute diffusion in the liquid, and triple-junction (TJ) are under non-equilibrium conditions is proposed for undercooled binary alloys. This model, compared with previous work, is applicable to concentrated alloys. Application of the model to the undercooled Ag–Cu eutectic alloy obtained a good agreement between model predictions and experimental results. An upper limit on the eutectic growth velocity is predicted above which migration of TJ is not kinetically possible and a transition from co-operative eutectic growth to single-phase growth occurs for concentrated alloys and dilute alloys with linear liquidus and solidus, respectively.

Introduction

Eutectic dendrite is a coupling microstructure. Its morphology as a whole is that of a dendrite, whereas its interface migration is dominated by co-operative growth of two or more solid phases [1–4]. The dendrite structure is formed by the well-known Mullins–Sekerka instability [5]. While taking a binary eutectic alloy as an example, one phase α repels the solute B while the other phase β repels the solvent A. Co-operative growth through solute diffusion in liquid results in the eutectic structure. If the Mullins–Sekerka instability [5] is introduced to eutectic interface, a eutectic dendrite structure is formed:

1. Addition of a third component. If both α and β reject the third component, its enrichment ahead of the interface results in a concentration gradient and then destabilization of the eutectic interface. Examples are the directional solidification of transparent ternary [1] and pseudo-ternary [2] eutectic alloys.
2. Eutectic growth in undercooled melts. In this case, both α and β reject latent heat into undercooled melts and the negative temperature gradient ahead of interface results in instability. Examples are rapid solidification of undercooled Co-Sb [3] and Co-Sn [4] eutectic alloys.

The recipe to model eutectic dendrite growth is to combine the eutectic growth model with the dendrite growth model. The pioneering work comes from Goetzinger–Barth–Herlach (GBH) [6]. They adopted the Zyrd–Gremaud–Kurz (ZGK) model [7] and the Lipton–Kurz–Trivedi (LKT) model [8] to describe solute diffusion parallel to interface and thermal diffusion perpendicular to interface, respectively. However, they used the exact solution of solute diffusion equation of Donaghey and Tiller [9] which was proposed for the linear phase diagram with constant solute partition coefficients $(k_{e\alpha}, k_{e\beta})$ and slopes of liquidus and solidus $(m^{e}_{L\alpha}, m^{e}_{L\beta}, m^{e}_{\alpha}, m^{e}_{\beta})$. Li and Zhou (LZ) [10] followed the Trivedi–Magnin–Kurz (TMK) model [11] in which the linear phase diagram is simplified to two types, i.e., one cigar-shaped in which the liquidus and solidus are parallel below the equilibrium eutectic temperature T^{e}_{E} and the other in

✉ Haifeng Wang
haifengw81@nwpu.edu.cn

Wangwang Kuang
kww@mail.nwpu.edu.cn

[1] State Key Laboratory of Solidification Processing, Northwestern Polytechnical University, Xi'an 710072, Shaanxi, People's Republic of China

[2] Institute of Problems of Chemical Physics, Academy of Sciences of Russia, Chernogolovka, Moscow Region, Russia 142432

which the equilibrium partition coefficients are constant and equal (i.e., $k_{e\alpha} = k_{e\beta} = k_e$). For both the GBH [6] and LZ [10] models, the eutectic dendrite in undercooled melts is assumed to be a thermal dendrite in which there exists only the curvature undercooling ΔT_R and the thermal undercooling ΔT_T. The effect of a third component on the eutectic dendrite growth was studied subsequently by Liu–Li–Zhou (LLZ) [12]. In this case, dendrite growth not only becomes thermal-controlled but also solute-controlled and there is an additional constitutional undercooling ΔT_C. Although progress has been made for modeling of eutectic dendrite growth [6, 10, 12], a comparative study between the predicted and measured growth velocity V as a function of undercooling ΔT is not satisfactory [4, 6, 13]. Further work needs to be done to take into account the four effects as follows.

1. Non-equilibrium interface kinetics. There are generally two independent dissipative processes at the interface, i.e., trans-interface diffusion and interface migration [14, 15]. The first solute redistribution process between solid and liquid corresponds to solute trapping [16, 17], that results in a deviation from the equilibrium concentrations. The second crystallization process results in deviation from the equilibrium temperature. The classical Jackson–Hunt (JH) [18] and TMK [11] models were proposed for solidification under local equilibrium conditions. For undercooled melts, the non-equilibrium interface kinetics can be so significant that it needs to be considered. For the case of equal kinetic partition coefficients $k_\alpha = k_\beta = k$, Kurz and Trivedi [19] substituted the kinetic slopes of liquidus $m_{L\alpha}$, $m_{L\beta}$ for $m^e_{L\alpha}$, $m^e_{L\beta}$ in the TMK model [11]. The kinetic undercooling ΔT_K was incorporated into the LZ [10] and LLZ [12] models but the non-equilibrium effects on the solute partition coefficients and slopes of liquidus were not taken into consideration. A complete description of non-equilibrium interface kinetics was conducted recently by Wang et al. [20, 21]; their model however is limited to dilute alloy systems.
2. Non-equilibrium solute diffusion (NESD). Practically, the measured growth velocity V [22] can be comparable with or even larger than the solute diffusion velocity in liquid, V_{DL}. In this case, solute diffusion is not only determined by its instantaneous concentration gradient but also relevant to its local history [23–27]. As a result, complete solute trapping (i.e., $k_\alpha = k_\beta = 1$) happens abruptly at a finite velocity $V = V_{DL}$. The NESD effect not only influences solute diffusion in bulk phases but also interface kinetics, as has been verified by experiments [24–27] and atomistic simulations [28]. Galenko and Herlach (GH) [29] solved the NESD equation of liquid in the case of $k_\alpha = k_\beta = k$, according to which they proposed a possible transition from eutectic solidification to partitionless solidification at $V = V_{DL}$.
3. Non-equilibrium triple-junction (TJ) kinetics. It can considerably influence the formation of eutectic patterns. One example is directional solidification of CBr_4–C_2Cl_6 eutectic system [30, 31]. Although the deviation of contact angles from the normal direction of eutectic interface is too small (e.g., 1°) to detect, its significant effect on stability is precisely measurable. Specific eutectic growth where both the α and β phases are stoichiometric compounds (SCs, $C_\alpha = \text{constant}$, $C_\beta = \text{constant}$) was studied recently [32]. In contrast to conventional understanding (e.g., Refs. [33, 34]), an exact solution of solute diffusion equation is available, in which the eutectic composition is necessarily found at TJ. The TJ kinetics could play such an important role in eutectic solidification [35] that it should be considered.
4. Concentrated alloys. The assumption of dilute alloys with linear liquidus and solidus prevails in the classical dendrite [8, 37] and eutectic [11, 18] growth models. These models are helpful to understand the solidification phenomena but may lead to significant deviation from the actual solidification process. The significant effects of non-linear liquidus and solidus, interaction between solute and solvent on interface kinetics [15, 38], stability of planar interface [39–41], and dendrite growth [42–44] have been studied recently. For dendritic solidification of one solid phase, dilute alloys may be possible but linear liquidus and solidus are applicable only to small values of ΔT [42], whereas for eutectic solidification of two or more solid phases, the assumption of dilute alloys with linear liquidus and solidus is actually not that practical.

In the current work, the non-equilibrium interface, TJ kinetics and NESD in liquid are integrated to propose a lamellar eutectic growth model. The model is then combined with the thermal dendrite growth [45, 46] model to obtain the current eutectic dendrite growth model. The eutectic dendrite growth model is applied to the undercooled Ag–Cu eutectic alloy which involves two solid solution phases (SSP). A good agreement between model predictions and experimental results [47] is obtained. The significant roles of the four effects abovementioned are shown and two new mechanisms for the upper limit of eutectic growth velocity are found.

Eutectic dendrite growth model

Let us start from lamellar eutectic growth under steady-state conditions (see Fig. 1a). First, a new solution of NESD equation in liquid in which kinetics of TJ is a

necessary boundary condition is derived. After that, the average interface kinetic condition [35] is formulated to uniquely determine the relation between the lamellar spacing λ and the interface undercooling ΔT_I ($= T_E^e - T_I$) for a given V by the minimum undercooling principle [18]. Finally, a negative temperature gradient is imposed to the growing lamellar eutectic interface to generate instability (Fig. 1b). The relation between the dendrite tip radius R and the thermal undercooling ΔT_T is determined uniquely for a given V by the thermal dendrite growth model of Galenko et al. [45, 46]. Noting that $\Delta T = \Delta T_I + \Delta T_T$, the current eutectic dendrite growth model is obtained by combining the lamellar eutectic model with the thermal dendrite growth model according to which λ, R, and ΔT are determined for a given V.

Solution of NESD equation in liquid

Attaching the co-ordinate system to the assumed planar interface (Fig. 1a), the NESD equation can be written as [29]

$$\frac{\partial^2 C_L}{\partial X^2} + \psi \frac{\partial^2 C_L}{\partial Z^2} + \frac{V}{D_L}\frac{\partial C_L}{\partial Z} = 0. \tag{1}$$

where C_L and D_L are the solute concentration and the diffusion coefficient in liquid, respectively. $\psi = 1 - V^2/V_{DL}^2$ is the relaxation factor as in Ref. [29]. The boundary conditions far away from the interface and the periodic conditions at the interface are

$$C_L = C_\infty \text{ at } Z = \infty, \tag{2}$$

$$\frac{\partial C_L}{\partial X} = 0 \text{ at } X = 0 \text{ and } X = S_\alpha + S_\beta, \tag{3}$$

where S_α and S_β are the half widths of the lamellae α and β, respectively. The solution of Eq. 1 with the boundary conditions Eqs. 2 and 3 is

$$C_L(X,Z) = \begin{cases} C_\infty + \sum_{n=0}^{\infty} B_n \cos(b_n X)\exp\left(-\frac{V}{D_L\psi}\omega_n Z\right), & V < V_{DL} \\ C_\infty, & V \geq V_{DL} \end{cases}, \tag{4}$$

where $b_n = 2n\pi/\lambda$ $(n = 0, 1, 2, \ldots)$ and $\omega_n = \left[1 + \sqrt{1 + \psi(2n\pi/P_e)^2}\right] \Big/ 2$ with $P_e = V\lambda/2D_L$ being the Peclet number. The Fourier coefficients B_n are evaluated from the average mass conservation law at the interface [32, 35]

$$-\frac{D_L\psi}{V}\left(\frac{\partial C_L}{\partial Z}\right)_{Z=0} = \begin{cases} \bar{C}^*_{L\alpha} - \bar{C}^*_{\alpha}, & 0 \leq X < S_\alpha \\ \bar{C}^*_{L\beta} - \bar{C}^*_{\beta}, & S_\alpha < X < S_\alpha + S_\beta \end{cases}, \tag{5}$$

where

$$\bar{C}^*_{L\alpha} = \frac{1}{S_\alpha}\int_0^{S_\alpha} C_L(X,0)\mathrm{d}X = C_\infty + B_0 + \sum_{n=1}^{\infty}\frac{B_n}{n\pi f_\alpha}\sin(n\pi f_\alpha), \tag{6}$$

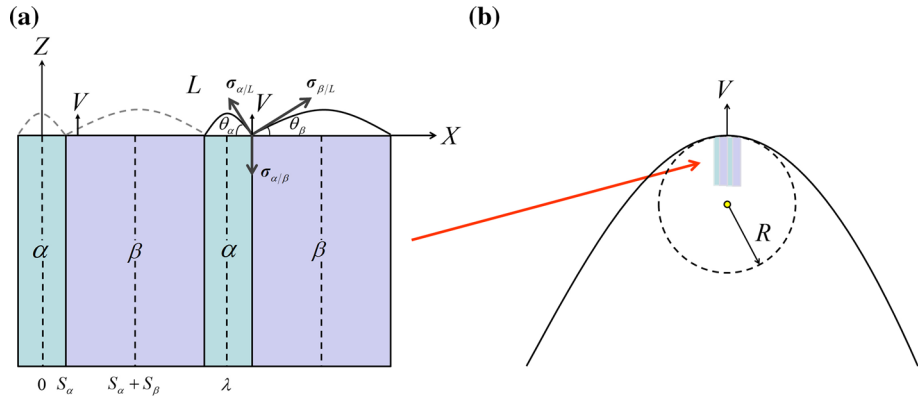

Fig. 1 Schematic diagram for modeling of eutectic dendrite growth in undercooled melts: lamellar eutectic (**a**) and eutectic dendrite (**b**) growth under steady-state conditions. Following the classical eutectic growth models [11, 18], a planar interface (**a**) is first assumed to obtain the solution of solute diffusion equation of liquid. Then, the interface kinetic conditions of the curved α/L and β/L interfaces are averaged to determine the unique relation between the lamellar spacing λ and the interface undercooling ΔT_I for a given velocity V by the minimum undercooling principle [18]. After that, a negative temperature gradient is imposed on the eutectic interface to generate its instability to dendrite growth (**b**). Because the dendrite tip radius R is several orders larger than the lamellar spacing λ (e.g., Fig. 5), the common method [6, 10, 12] to combine the eutectic growth with the dendrite growth model is adopted to formulate the current model. For eutectic growth, not only lateral but longitudinal diffusion is also limited to the length scale of lamellar spacing; please see, e.g., Figures 2 and B1 in Ref. [32]. This is the reason why the eutectic dendrite is approximated as a purely thermal dendrite [6, 10] even if there is solute diffusion in liquid

$$\bar{C}^*_{\mathrm{L}\beta} = \frac{1}{S_\beta}\int_{S_\alpha}^{S_\alpha+S_\beta} C_{\mathrm{L}}(X,0)\mathrm{d}X = C_\infty + B_0 - \sum_{n=1}^{\infty}\frac{B_n}{n\pi f_\beta}\sin(n\pi f_\alpha), \tag{7}$$

are the average liquid concentrations at the α/L and β/L interfaces, $\bar{C}^*_\alpha$, $\bar{C}^*_\beta$ are the corresponding average solid concentrations, and '*' denotes the value at the interface. Substituting Eqs. 4, 6, and 7 into Eq. 5 yields

$$C_\infty = f_\alpha \bar{C}^*_\alpha + f_\beta \bar{C}^*_\beta, \tag{8}$$

$$B_n = \frac{2\sin(n\pi f_\alpha)}{\omega_n n\pi}\left(\bar{C}^*_\beta - \bar{C}^*_\alpha\right)\Bigg/\left[1 - \sum_{m=1}^{\infty}\frac{2\sin^2(m\pi f_\alpha)}{\omega_m m^2\pi^2 f_\alpha f_\beta}\right] \ (n \geq 1), \tag{9}$$

where f_α and f_β are the volume fractions of lamellas α and β. Compared with the JH [18], DT [9], and TMK [11] solutions, it is the global mass conservation law (Eq. 8), but not the Fourier coefficient B_0 that is obtained. Therefore, one more boundary condition is needed, which is the "extrinsic" kinetics of TJ [32, 36]

$$C^*_{\mathrm{L}}|_{X=S_\alpha} = C^\wedge_{\mathrm{L}} = C^{\mathrm{ne}}_{\mathrm{EL}}. \tag{10}$$

Combining of Eq. 4 with Eq. 10, B_0 is expressed as

$$B_0 = C^\wedge_{\mathrm{L}} - C_\infty - \sum_{n=1}^{\infty} B_n\cos(n\pi f_\alpha). \tag{11}$$

In contrast to our understanding from textbooks [33, 34], the kinetic eutectic composition $C^{\mathrm{ne}}_{\mathrm{EL}}$ is necessarily found at the TJ and it can be obtained from the following equations [35]:

$$\frac{V}{V^{\mathrm{I}}_{\mathrm{DL}}} = \frac{R_{\mathrm{g}}T_{\mathrm{I}}}{C^\wedge_{\mathrm{L}} - C^\wedge_\alpha}\left(\frac{\partial\tilde{\mu}^\wedge_{\mathrm{L}}}{\partial C^\wedge_{\mathrm{L}}}\right)^{-1}\psi\left[1 - \exp\left(\frac{\Delta\mu^{A\wedge}_{\alpha/\mathrm{L}} - \Delta\mu^{B\wedge}_{\alpha/\mathrm{L}}}{R_{\mathrm{g}}T_{\mathrm{I}}}\right)\right], \tag{12}$$

$$\frac{V}{V^{\alpha/\mathrm{L}}_0} = 1 - \exp\left[\frac{C^\wedge_{\mathrm{L}}\Delta\mu^{B\wedge}_{\alpha/\mathrm{L}} + \left(1 - C^\wedge_{\mathrm{L}}\right)\Delta\mu^{A\wedge}_{\alpha/\mathrm{L}}}{R_{\mathrm{g}}T_{\mathrm{I}}}\right], \tag{13}$$

$$\frac{V}{V^{\mathrm{I}}_{\mathrm{DL}}} = -\frac{R_{\mathrm{g}}T_{\mathrm{I}}}{C^\wedge_{\mathrm{L}} - C^\wedge_\beta}\left(\frac{\partial\tilde{\mu}^\wedge_{\mathrm{L}}}{\partial C^\wedge_{\mathrm{L}}}\right)^{-1}\psi\left[1 - \exp\left(\frac{\Delta\mu^{B\wedge}_{\beta/\mathrm{L}} - \Delta\mu^{A\wedge}_{\beta/\mathrm{L}}}{R_{\mathrm{g}}T_{\mathrm{I}}}\right)\right], \tag{14}$$

$$\frac{V}{V^{\beta/\mathrm{L}}_0} = 1 - \exp\left[\frac{C^\wedge_{\mathrm{L}}\Delta\mu^{B\wedge}_{\beta/\mathrm{L}} + \left(1 - C^\wedge_{\mathrm{L}}\right)\Delta\mu^{A\wedge}_{\beta/\mathrm{L}}}{R_{\mathrm{g}}T_{\mathrm{I}}}\right]. \tag{15}$$

where the superscript '^' denotes the values at TJ, $V^{\mathrm{I}}_{\mathrm{DL}}$ is the solute diffusion velocity of interface, $V^{i/j}_0$ is the upper limit velocity for the migration of i/j interface, μ_i is the chemical potential, and $\tilde{\mu}_i = \mu^B_i - \mu^A_i$ is the solute diffusion potential for the i component, $\Delta\mu^{B\wedge}_{i/j} = \mu^{B\wedge}_i - \mu^{B\wedge}_j$, $\Delta\mu^{A\wedge}_{i/j} = \mu^{A\wedge}_i - \mu^{A\wedge}_j$, R_{g} is the gas constant, and T_{I} is the interface temperature. A comparative study between the solutions with and without TJ kinetics was carried out in Ref. [32]. The current solution is an extension of previous solution [32, 35] to the case of NESD and in comparison to the GH solution [29], is applicable to concentrated alloys.

Average interface conditions and lamellar spacing

In the case of linear liquidus and solidus, the average interface undercoolings of α/L and β/L interfaces are averaged again by the slopes of equilibrium [6, 10–12, 18] or non-equilibrium [19] liquidus of α and β phases. This treatment is not convenient here because the interface undercooling contributions ΔT_{C}, ΔT_{R}, and ΔT_{K} cannot be obtained analytically in the case of non-linear liquidus and solidus. Therefore, the average interface kinetic conditions for migration of α/L and β/L interfaces are averaged by the volume fractions of α and β phases [35].

$$V = \sum_{i=\alpha,\beta} f_i V_0^{i/\mathrm{L}}\left\{1 - \exp\left[\frac{\bar{C}^*_{Li}\Delta\bar{\mu}^{B*}_{i/\mathrm{L}} + \left(1 - \bar{C}^*_{Li}\right)\Delta\bar{\mu}^{A*}_{i/\mathrm{L}} - V_m\bar{K}_{i/\mathrm{L}}\sigma_{i/\mathrm{L}}}{R_{\mathrm{g}}T_{\mathrm{I}}}\right]\right\}. \tag{16}$$

where $\sigma_{i/\mathrm{L}}$ is the interface tension for i/L interface. The average curvature $\bar{K}_{i/\mathrm{L}}$ is [18][1]:

$$-\bar{K}_{i/\mathrm{L}} = \frac{2\sin\theta_i}{\lambda f_i} \quad (i = \alpha, \beta). \tag{17}$$

The contact angles θ_α and θ_β are obtained from the "intrinsic" kinetics of TJ [35], which in the case of 1-D steady-state growth reduce to

$$\begin{aligned}&\sigma_{\alpha/\mathrm{L}}\cos\theta_\alpha - \sigma_{\beta/\mathrm{L}}\cos\theta_\beta = 0,\\ &V = M_{\mathrm{TJ}}\left(\sigma_{\alpha/\mathrm{L}}\sin\theta_\alpha + \sigma_{\beta/\mathrm{L}}\sin\theta_\beta - \sigma_{\alpha/\beta}\right).\end{aligned} \tag{18}$$

The averaged interface kinetic conditions for trans-interface diffusion are [35]

$$\frac{V}{V^{\mathrm{I}}_{\mathrm{DL}}} = \frac{R_{\mathrm{g}}T_{\mathrm{I}}}{\bar{C}^*_{\mathrm{L}\alpha} - \bar{C}^*_\alpha}\left(\frac{\partial\bar{\tilde{\mu}}^*_{\mathrm{L}}}{\partial\bar{C}^*_{\mathrm{L}\alpha}}\right)^{-1}\psi\left[1 - \exp\left(\frac{\Delta\bar{\mu}^{A*}_{\alpha/\mathrm{L}} - \Delta\bar{\mu}^{B*}_{\alpha/\mathrm{L}}}{R_{\mathrm{g}}T_{\mathrm{I}}}\right)\right], \tag{19}$$

$$\frac{V}{V^{\mathrm{I}}_{\mathrm{DL}}} = -\frac{R_{\mathrm{g}}T_{\mathrm{I}}}{\bar{C}^*_{\mathrm{L}\beta} - \bar{C}^*_\beta}\left(\frac{\partial\bar{\tilde{\mu}}^*_{\mathrm{L}}}{\partial\bar{C}^*_{\mathrm{L}\beta}}\right)^{-1}\psi\left[1 - \exp\left(\frac{\Delta\bar{\mu}^{B*}_{\beta/\mathrm{L}} - \Delta\bar{\mu}^{A*}_{\beta/\mathrm{L}}}{R_{\mathrm{g}}T_{\mathrm{I}}}\right)\right]. \tag{20}$$

[1] At the tip of eutectic dendrite, $-\bar{K}_{i/\mathrm{L}} = 2\sin\theta_i/\lambda f_i + 2/R$ is obtained where the first and the second term on the right-hand side are the contributions from the eutectic and dendrite structures, respectively. However, R is several orders larger than λ (Fig. 5) and thus it is advisable to omit the second term.

The relation between λ and ΔT_{I} can be determined uniquely for a given V if the minimum undercooling principle [18] is assumed to be the operation point of eutectic growth:

$$\frac{\partial \Delta T_{\mathrm{I}}}{\partial \lambda} = 0. \tag{21}$$

Thermal dendrite growth and dendrite tip radius

For a purely thermal-controlled dendrite growth, ΔT_{T} can be obtained from the Ivantsov solution [8, 37] as

$$\Delta T_{\mathrm{T}} = \frac{\Delta \bar{H}_{\mathrm{f}}}{\bar{C}_{\mathrm{P}}^{\mathrm{L}}} \mathrm{Iv}(P_{\mathrm{T}}), \tag{22}$$

where $\Delta \bar{H}_{\mathrm{f}}$ $(= f_\alpha \Delta \bar{H}_{\mathrm{f}}^{\alpha} + f_\beta \Delta \bar{H}_{\mathrm{f}}^{\beta})$ is the average latent heat of fusion, $\bar{C}_{\mathrm{P}}^{\mathrm{L}}$ $(= f_\alpha \bar{C}_{\mathrm{P}}^{\mathrm{L}\alpha} + f_\beta \bar{C}_{\mathrm{P}}^{\mathrm{L}\beta})$ is the average specific heat of undercooled melts, $P_{\mathrm{T}} = VR/2\alpha_{\mathrm{L}}$ with α_{L} the thermal diffusion coefficient is the thermal Peclet number. Equation 22 gives a relation between VR and ΔT_{T}. To find a unique solution, a second equation is needed, e.g., from the solvability theory [45, 46]:

$$R = \left(\frac{\bar{\Gamma}}{\sigma_0 \varepsilon^{7/4}}\right) \Big/ \left[P_{\mathrm{T}} \Delta \bar{H}_{\mathrm{f}} \xi_{\mathrm{T}} / 2\bar{C}_{\mathrm{P}}^{\mathrm{L}}\right], \tag{23}$$

where $\xi_{\mathrm{T}} = 1/\left(1 + a_{\mathrm{T}} \varepsilon P_{\mathrm{T}}^2\right)$, $\bar{\Gamma}$ $(= f_\alpha \bar{\Gamma}_{\mathrm{L}\alpha} + f_\beta \bar{\Gamma}_{\mathrm{L}\beta}$, where $\bar{\Gamma}_{Li} = \sigma_{i/\mathrm{L}} V_m / \Delta \bar{S}_{\mathrm{f}}^{i}$ and $\Delta \bar{S}_{\mathrm{f}}^{i}$ is the average entropy of fusion of the i/L interface) is the average Gibbs–Thompson coefficient, ε is the anisotropy coefficient, $\sigma_0 = 1/0.42$ and $a_{\mathrm{T}} = 0.3$. For a given V, R, and ΔT_{T} can be determined by Eqs. 22 and 23.

Until now, the eutectic dendrite growth model for undercooled binary alloy has been developed. One can obtain λ, R, and ΔT for a given V by integrating Eqs. 6–9 and 11–23. The current work in comparison with the previous eutectic dendrite growth models [6, 10, 12] can be summarized as follows. (1) The non-equilibrium interface, TJ kinetics, NESD, and its effect on the interface kinetics are integrated. (2) It is applicable to a concentrated alloy system. A simplification to the case of dilute alloys with linear liquidus and solidus is given in Appendix.

Application to undercooled Ag–Cu eutectic alloy

The current model was applied to undercooled Ag–Cu eutectic alloy. The thermodynamic assessment by Subramanlan and Perepezko [48] was applied to obtain the thermodynamic properties μ_i^A, μ_i^B, $\Delta H_{\mathrm{f}}^{i}$, C_{P}^{Li}, and $\Delta S_{\mathrm{f}}^{i}$ $(i = \alpha, \beta$ denote, respectively, the Ag and Cu phases). Accordingly, we have $T_{\mathrm{E}}^{\mathrm{e}} = 1053.7\,\mathrm{K}$, $C_{\mathrm{EL}}^{\mathrm{e}} = 0.3944$, $C_{\mathrm{E}\alpha}^{\mathrm{e}} = 0.136$, $C_{\mathrm{E}\beta}^{\mathrm{e}} = 0.952$, $T_m^{\mathrm{Ag}} = 1235.3\,\mathrm{K}$, and $T_m^{\mathrm{Cu}} = 1357\,\mathrm{K}$ from the equilibrium phase diagram; please see the solid lines in Fig. 8a. Other physical parameters used are summarized in Table 1.

Table 1 Physical parameters for simulation of undercooled Ag–Cu eutectic alloy

Parameters	Values
$V_{\mathrm{DL}}^{\mathrm{I}}$ (m s^{-1})	0.526
V_{DL} (m s^{-1})	1
$V_0^{\alpha/\mathrm{L}}$ (m s^{-1})	100
$V_0^{\beta/\mathrm{L}}$ (m s^{-1})	100
D_{L} (m^2 s^{-1})	3.8×10^{-9}
M_{TJ} (m^3 J^{-1} s^{-1})	2
α_{L} (m^2 s^{-1})	3×10^{-6}
V_m (m^3 mol^{-1})	7.58×10^{-6}
$\sigma_{\alpha/\mathrm{L}}$ (J m^{-2})	0.3
$\sigma_{\beta/\mathrm{L}}$ (J m^{-2})	0.5
ε (–)	0.0078

A fluxing melt technique was applied to undercool the Ag–Cu eutectic alloy, and a high-speed camera was used to record the propagation of recalescence fronts by Clopet et al. [47]. Figure 2 shows a comparison between model predictions and experimental results for the $V \sim \Delta T$ relation. The current model (the solid line) reproduces the experimental results well except for the data point at $\Delta T = 60$ K.[2] Although Clopet et al. [47] believed that the sharp decrease of V at $\Delta T = 60$ K is real, it cannot be predicted currently. We would like to note that if the mobility for interface migration and solute diffusion coefficient are temperature dependent, a transition from thermodynamics-controlled to kinetics-controlled growth happens and a first increase of V with ΔT is followed by a decrease [35, 49]; such transition, however, happens at very large ΔT.

Figure 3 shows the evolutions of ΔT_{T} and ΔT_{I} with ΔT. ΔT_{T} is dominated at low and medium ΔT, whereas with

[2] It must be pointed out that breakdown of eutectic growth to single dendrite growth happens at $\Delta T \approx 70$ K according to the experimental results of Clopet et al. [47]. Similar result was also found by Wang and Herlach [50, 51] and Zhao et al. [52, 53] and was ascribed to the limit of T_0 line. For such small undercooling $\Delta T < 70$ K, the non-equilibrium effects are actually negligible. According to the current model prediction, however, eutectic growth holds until an upper limit of eutectic growth velocity $V = 0.177$ m s^{-1} where $\Delta T = 350$ K is much higher than 70 K; please see the extended dashed line in Fig. 2. Regarding that eutectic growth always holds through the whole experimentally accessible undercooling for some alloys, e.g., Fe–B [36], Ni–Sn [13], extension of current model prediction to high undercooling may be helpful to show at least qualitatively the non-equilibrium effects during rapid eutectic growth as well as the effect of concentrated alloys.

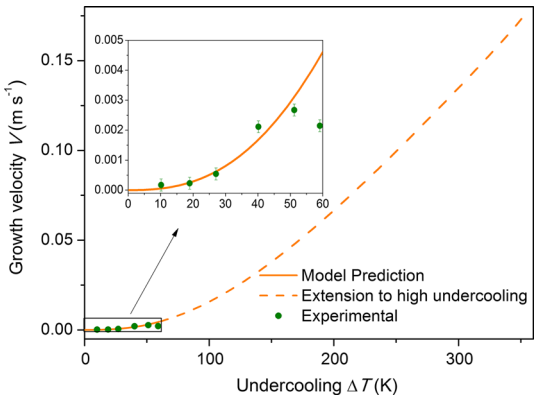

Fig. 2 The growth velocity V as a function of undercooling ΔT: current model predictions, the *solid line*; extension of the model predictions to high undercooling, the dashed line; experimental results of Clopet et al. [53], the *solid circles*

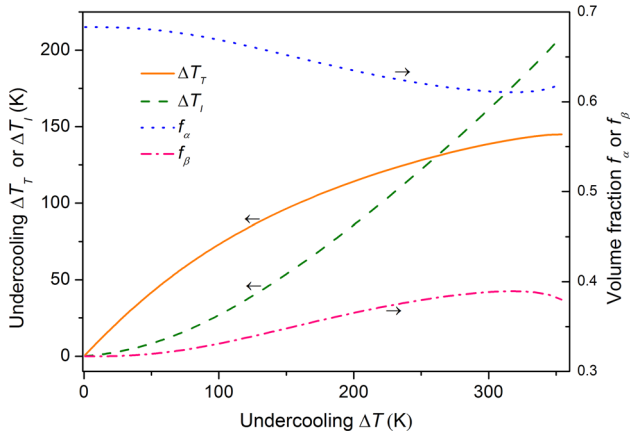

Fig. 3 The undercooling contributions (the thermal undercooling ΔT_{T}, the *solid line*; the interface undercooling ΔT_{I}, the *dashed line*) and the volume fractions (of the α phase f_α, the *dotted line*; of the β phase, the *dash-dotted line*) as a function of undercooling ΔT

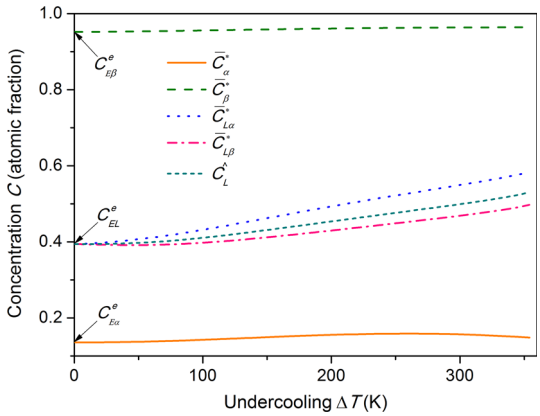

Fig. 4 The average solid, liquid concentrations at the α/L, β/L interfaces ($\bar{C}^*_\alpha$, the *solid line*; $\bar{C}^*_\beta$, the *dashed line*; $\bar{C}^*_{L\alpha}$, the *dotted line*; $\bar{C}^*_{L\beta}$, the *dash-dotted line*) and the concentration at TJ ($C^\wedge_{\mathrm{L}}$, the *short-dashed line*) as a function of undercooling ΔT

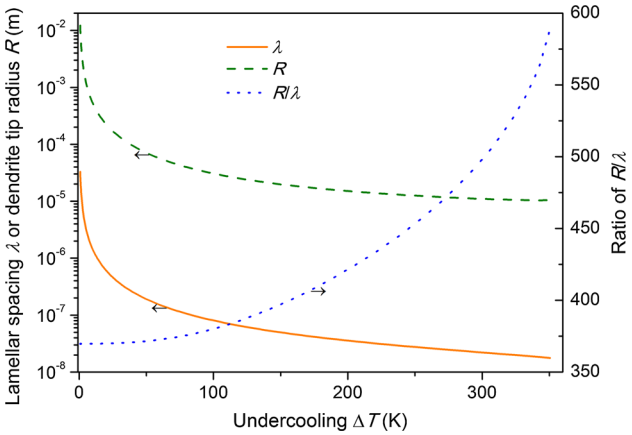

Fig. 5 The lamellar spacing λ (the *solid line*), the dendrite tip radius R (the *dashed line*) and their ratio R/λ (the *dotted line*) as a function of undercooling ΔT

further increase of ΔT, there is a faster increase of ΔT_{I} resulting in ΔT_{I} being larger than ΔT_{T}. This suggests that non-equilibrium interface kinetics plays an important role at high ΔT. Because it is not possible to distinguish ΔT_{C}, ΔT_{K}, and ΔT_{R} from ΔT_{I} in the case of concentrated alloys, evolutions of the average concentrations at the α/L, β/L interfaces ($\bar{C}^*_\alpha$, $\bar{C}^*_\beta$, $\bar{C}^*_{\mathrm{L}\alpha}$, $\bar{C}^*_{\mathrm{L}\beta}$) and the concentration at the TJ ($C^\wedge_{\mathrm{L}} = C^{\mathrm{ne}}_{\mathrm{EL}}$) with ΔT are calculated (Fig. 4). At small ΔT, $\bar{C}^*_\alpha = C^{\mathrm{e}}_{\mathrm{E}\alpha}$, $\bar{C}^*_\beta = C^{\mathrm{e}}_{\mathrm{E}\beta}$ and $\bar{C}^*_{L\alpha} = \bar{C}^*_{\mathrm{L}\beta} = C^\wedge_{\mathrm{L}} = C^{\mathrm{e}}_{\mathrm{EL}}$. The local equilibrium conditions hold at not only interfaces but also at TJ. The liquid concentration at the interface can approximately be given as the equilibrium eutectic composition (i.e., $C^*_{\mathrm{L}} = C^{\mathrm{e}}_{\mathrm{EL}}$) (e.g., the JH model [18]). With an increase in ΔT, $\bar{C}^*_\alpha$, $\bar{C}^*_\beta$, $\bar{C}^*_{\mathrm{L}\alpha}$, $\bar{C}^*_{\mathrm{L}\beta}$, and $C^\wedge_{\mathrm{L}}$ deviate gradually from their equilibrium values. The concentrations are varied along the interface and their deviation from the local equilibrium conditions are so significant that not only JH [18] but even TMK [11] models are inapplicable. A result of evolutions of $\bar{C}^*_\alpha$ and $\bar{C}^*_\beta$ with ΔT is the corresponding variation of f_α and f_β due to the global mass conservation law Eq. 8; denoted by the dotted and dash-dotted lines in Fig. 3. In other words, the non-equilibrium effects influence not only the eutectic growth kinetics but also the volume fractions of the lamellae.

Evolutions of λ, R, and their ratio R/λ with ΔT are shown in Fig. 5. The extremely large ratio of R/λ implies that the dendrite can be taken as a planar interface at the tip compared with the lamellar spacing. Therefore, a direct combination of lamellar eutectic growth with thermal dendrite growth that occurs at different length scales is a reasonable recipe [10].

Discussion

Effect of concentrated alloys

Most of the previous eutectic growth models are established for dilute alloys with linear liquidus and solidus, e.g., Refs. [6, 7, 9–12, 18, 19]. For an actual eutectic alloy, the liquidus and solidus are non-linear and the interaction between the solute and the solvent is not negligible anymore. A comparison between the models for concentrated alloys and dilute alloys with linear liquidus and solidus is shown in Fig. 6. The $\Delta T \sim V$ relations are indistinguishable for $\Delta T < 100$ K and difference between them becomes significant with further increase of ΔT. The $\lambda \sim V$ relations are the same at small V and the differences between them are not too large even at large V. This means that the assumption of dilute alloys with linear liquidus and solidus is only applicable to small V (ΔT). The significant deviation at large V (ΔT) clearly shows the necessity to propose the current model for concentrated alloys. Note that for both cases, there is a critical velocity above which cooperative eutectic growth cannot hold; please see our discussion in the following sections.

Effect of non-equilibrium kinetics

For eutectic growth in undercooled melts, the interface, TJ, and solute diffusion in liquid are under local non-equilibrium conditions. To show their respective effects, different combinations of non-equilibrium kinetics are adopted to calculate the model for dilute alloys with linear liquidus and solidus; please see Fig. 7a, b. Let us first consider the case with all of the three types of non-equilibrium effects: $C_L^{\wedge} = C_{EL}^{ne}$ (non-equilibrium interface and "extrinsic" TJ kinetics), $V_{DL} = 1$ m s^{-1} (a finite value of V_{DL} corresponds to NESD), and $M_{TJ} = 2$ m^4 J^{-1} s^{-1} (a finite value of M_{TJ} corresponds to "intrinsic" TJ kinetics [35]). The predicted $\Delta T \sim V$ and $\lambda \sim V$ relations are shown as the solid lines in Fig. 7.

Then, we set $M_{TJ} \to \infty$, so that is there is no "intrinsic" TJ kinetics; please see the dashed lines in Fig. 7. Compared to the first case, both ΔT and λ becomes larger at high V, suggesting that the TJ kinetic effect could be significant. Let us further set $V_{DL} \to \infty$, that is, solute diffusion in liquid is under local equilibrium conditions; please see the dotted line in Fig. 7. A comparison between the second and third cases shows that NESD does not have a significant effect on ΔT and λ even at high V. In contrast to GH [29], a complete eutectic growth model is derived currently. Our simulation results, however, show that the NESD effect is not that important compared to dendrite growth upon

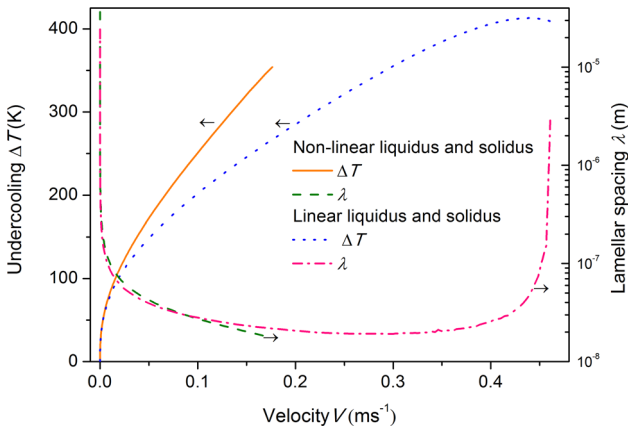

Fig. 6 The undercooling ΔT and lamellar spacing λ as a function of the growth velocity V for the cases of concentrated alloys (the *solid* and *dashed lines*) and dilute alloys with linear liquidus and solidus (the *dotted* and *dash-dotted lines*)

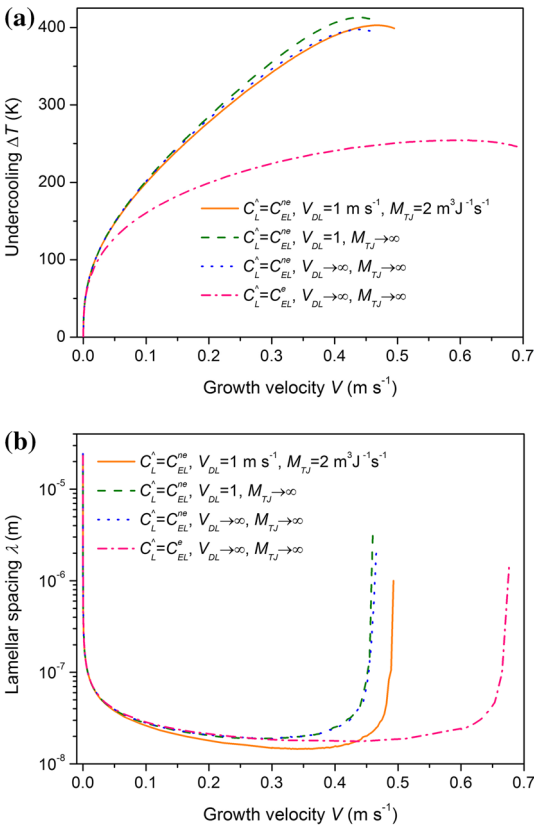

Fig. 7 The undercooling ΔT (**a**) and the lamellar spacing λ (**b**) as a function of the growth velocity V for different combinations of non-equilibrium kinetics. The concentration at the TJ $C_L^{\wedge}$ equals the kinetic eutectic composition C_{EL}^{ne} (or the equilibrium eutectic composition C_{EL}^{e}), meaning there is a (or is no) non-equilibrium interface and "extrinsic" TJ kinetics. A finite $V_{DL} = 1$ m s^{-1} (or an infinite $V_{DL} = \infty$) implies that solute diffusion in liquid is (or is not) under local non-equilibrium conditions. A finite $M_{TJ} = 2$ m^3 J^{-1} s^{-1} (or an infinite $M_{TJ} = \infty$) means that there is (or is no) non-equilibrium "intrinsic" kinetics of TJ

which a transition to partitionless solidification is followed by a change of growth mechanism from a power law to a linear law at $V = V_{DL}$ [26, 27, 42–44]. The reason is that for both the concentrated and dilute alloys, co-operative eutectic growth fails when V is much smaller than V_{DL}; please see Figs. 6 and 7. Finally, we set $C_L^{\wedge} = C_{EL}^{e}$, that is, there are no interface and "extrinsic" TJ kinetics [36]. In this case, the interface, TJ and solute diffusion in liquid are all under local equilibrium conditions. The extreme deviations from the above three cases for ΔT when $V > 0.05$ m s^{-1} and λ when $V > 0.35$ m s^{-1} show the important roles of non-equilibrium interface and "extrinsic" TJ kinetics. In one word, the effects of concentrated alloys, non-equilibrium interface ,and TJ kinetics play important roles in eutectic growth but not the NESD effect.

Upper limit of eutectic growth velocity

Two different mechanisms are given by TMK [11]. One is the temperature-dependent diffusion coefficient that leads to a transition from thermodynamics-controlled to kinetics-controlled growth [35, 49]. The other is the limit of undercooling constrained by the phase diagram. If the interface temperature reaches the solidus temperature for a given phase, a transition from co-operative eutectic growth to single-phase growth happens. In the current work, an upper limit of eutectic growth velocity is found for both concentrated and dilute alloys (Figs. 6, 7). The physics behind each case is, however, different from TMK [11].

Co-operative eutectic growth occurs by migration of TJ at which two or more solids are solidified simultaneously from one liquid. Therefore, eutectic growth can occur only when migration of TJ is kinetically possible. Figure 8a shows the kinetic phase diagrams of concentrated Ag–Cu eutectic alloy. The equilibrium phase diagram ($V = 0$) is shown as the solid lines. With the increase of V, the absolute value of the slope of liquidus increases and that of solidus decreases, e.g., the dashed lines for $V = 0.1$ m s^{-1}. The kinetic liquidus of Ag and Cu phases interact with each other at a kinetic eutectic point. However, when V increases to a critical value $V = 0.177$ m s^{-1}, there is no kinetic eutectic point anymore. Taking $V = 0.18$ m s^{-1} as an example, the kinetic liquidus and solidus temperatures of the Cu phase decrease gradually with the decrease of Cu composition, whereas for the Ag phase, they first decrease and then increase again with the decrease of Ag composition; please see the dotted lines. For the case of $V = 0.4$ m s^{-1}, there is no kinetic eutectic point because the kinetic liquidus and solidus of the Ag phase interacts with each other primarily; please see the dash-dotted lines. When $V \geq V_{DL} = 1$ m s^{-1}, complete solute trapping happens and the kinetic liquidus and solidus of the Ag and Cu phases coincide with each other; please see the short-dashed ($V = 1$ m s^{-1}) and short-dotted ($V = 2$ m s^{-1}) lines. In this case, the Ag phase does not repel Cu atoms and the Cu phase does not repel Ag atoms. Co-operative eutectic growth through solute diffusion in liquid fails completely. In short, there is a critical velocity above which there is no kinetic eutectic point and the upper limit of eutectic growth velocity is constrained by the "extrinsic" TJ kinetics. Evolutions of C_{EL}^{ne} and T_E^{ne} with V are summarized in Fig. 8b. The considerable deviations of C_{EL}^{ne} and C_{EL}^{ne} from C_{EL}^{e} and T_E^{e} again highlight the need to incorporate non-equilibrium kinetics into current work.

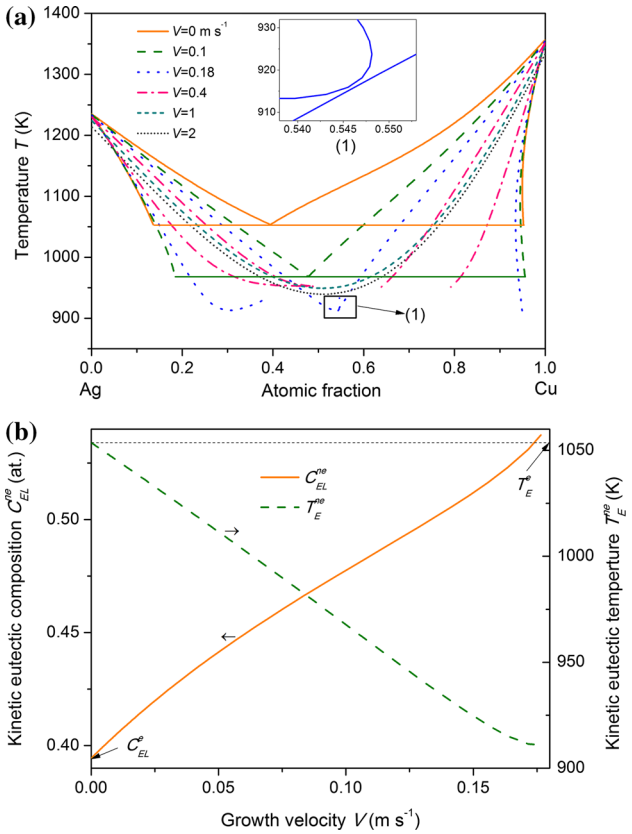

Fig. 8 The kinetic phase diagrams of concentrated Ag–Cu eutectic alloy (**a**) and the corresponding kinetic eutectic composition C_{EL}^{ne} (the *solid line*) and temperature T_E^{ne} (the *dashed line*) as a function of the growth velocity V (**b**)

For dilute alloys with linear liquidus and solidus, the absolute value of the slope of liquidus increases and that of solidus decreases continuously with V until they coincide at $V = V_{DL}$. Because the kinetic liquidus and solidus hold as linear lines in the kinetic phase diagrams, there is always a kinetic eutectic point for $V < V_{DL}$. The upper limit of eutectic growth velocity was regarded to be the solute diffusion velocity in liquid V_{DL} [29], which is however not the case; please see Fig. 7. Because the $\Delta T \sim V$ and $\lambda \sim V$ relations are similar for all of the four cases, the upper limit of eutectic growth velocity is independent of the non-equilibrium effects.

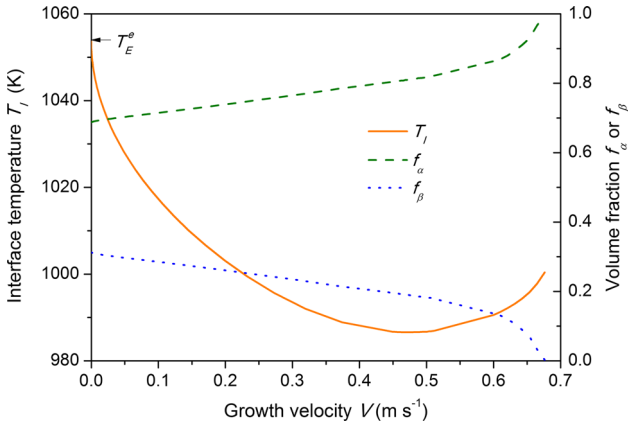

Fig. 9 The interface temperature T_I (the *solid line*), volume fractions of α, β phases f_α (the *dashed line*), f_β (the *dotted line*) as a function of the growth velocity V for the case of dilute alloys with linear liquidus and solidus

In the original JH model [18], it was found that an appreciable change in the ratio of lamellar spacing S_β/S_α negligibly changes eutectic growth kinetics. Therefore, f_α and f_β are assumed to be constants, which followed from all of the previous eutectic growth models [6, 7, 10–12, 18–21]. In the current work, the incorporation of TJ kinetics spontaneously releases this assumption. f_α and f_β are not given for the model simulations but are the simulation results; please see Fig. 3. Let us now consider a special case without non-equilibrium kinetics; please see the dash-dotted lines in Fig. 7. Evolutions of f_α and f_β are shown as the dashed and dotted lines in Fig. 9. f_α increases gradually to 1 whereas f_β decreases gradually to 0 with the increase of V. At the critical velocity $V = 0.677$ m s^{-1}, a transition from eutectic growth to single-phase growth happens. This mechanism may seem similar to but is actually different from the second mechanism of TMK [11]. First, $k_{e\alpha} = 0.345$ and $k_{e\beta} = 0.079$ are not close to 1. Second, the minimum interface undercooling 986.57 K is much larger than the solidus temperature of Ag 708.66 K in the linear phase diagram; please see the solid line in Fig. 9.

Conclusions

In this paper, a eutectic dendrite growth model is developed for the undercooled binary alloys and applied to the undercooled Ag–Cu eutectic alloy. Our main conclusions are as follows.

1. The model is applicable to concentrated eutectic alloys and a good agreement between model predictions and experimental results is obtained for the undercooled Ag–Cu eutectic alloy. The effects of concentrated alloys, non-equilibrium interface, and TJ kinetics play important roles but not the NESD effect because the upper limit of eutectic growth velocity is much smaller than the solute diffusion velocity in liquid.
2. The incorporation of TJ kinetics into the current model results in two new mechanisms for the upper limit of eutectic growth velocity. One is that migration of TJ could not be kinetically possible and the other is that a transition from co-operative eutectic to single-phase growth happens at high V. In contrast to GH [29], who proposed a possible transition from eutectic solidification to partitionless solidification from their solution of NESD equation for a liquid, our work shows that eutectic growth fails already before the occurrence of partitionless solidification.

Further work needs to be carried out because the experimentally observed sharp decrease of V at $\Delta T = 60$ K and breakdown of eutectic growth to single dendrite growth at $\Delta T \approx 70$ K cannot be predicted currently for the undercooled Ag–Cu eutectic alloy.

Acknowledgements The authors are grateful to the National Basic Research Program of China (973 Program, No. 2011CB610403), the National Science Funds for Distinguished Young Scientists (No. 51125002), the Natural Science Foundation of China (Nos. 51371149 and 51101122), and the Free Research Fund of State Key Lab. of Solidification Processing (No. 92-QZ-2014), Fundamental Research Funds for the Central Universities (No. 3102015AX0003), Shaanxi Young Stars of Science and Technology (No. 2015KJXX-10). Wangwang Kuang thanks the Graduate Starting Seed Fund of Northwestern Polytechnical University (No. 2013200632).

Appendix

Dilute alloys with linear liquidus and solidus

In the case of linear liquidus and solidus, the equilibrium concentrations C_α^e, $C_{L\alpha}^e$, C_β^e, and $C_{L\beta}^e$ at the eutectic temperature can be expressed as

$$C_\alpha^e = \frac{T_I - T_m^A}{m_{L\alpha}^e} k_{e\alpha},\ C_{L\alpha}^e = \frac{T_I - T_m^A}{m_{L\alpha}^e},$$
$$C_\beta^e - 1 = \frac{T_I - T_m^B}{m_{L\beta}^e} k_{e\beta},\ C_{L\beta}^e - 1 = \frac{T_I - T_m^B}{m_{L\beta}^e}, \quad (24)$$

where

$$k_{e\alpha} = \frac{C_\alpha^e}{C_{L\alpha}^e},\ k_{e\beta} = \frac{1 - C_\beta^e}{1 - C_{L\beta}^e}, \quad (25)$$

are the equilibrium partition coefficients and,

$$T_m^A = T_E^e - m_{L\alpha}^e C_{EL}^e,\ T_m^B = T_E^e + m_{L\beta}^e \left(1 - C_{EL}^e\right), \quad (26)$$

are the melting temperatures of pure A and B. For dilute alloys in which the interaction between solute and solvent is negligible, the chemical potentials follow Henry's law

$$\Delta\mu_{i/\mathrm{L}}^{A*} = R_\mathrm{g}T_\mathrm{I}\ln\frac{\left(1-C_i^*\right)\left(1-C_{Li}^\mathrm{e}\right)}{\left(1-C_\mathrm{L}^*\right)\left(1-C_i^\mathrm{e}\right)},$$
$$\Delta\mu_{i/\mathrm{L}}^{B*} = R_\mathrm{g}T_\mathrm{I}\ln\frac{C_i^*C_{Li}^\mathrm{e}}{C_\mathrm{L}^*C_i^\mathrm{e}} \quad (i=\alpha,\beta), \tag{27}$$

$$\frac{\partial\tilde{\mu}_\mathrm{L}^*}{\partial C_\mathrm{L}^*} = \frac{R_\mathrm{g}T_\mathrm{I}}{C_\mathrm{L}^*\left(1-C_\mathrm{L}^*\right)}. \tag{28}$$

For the α phase, Eq. 27 can be reformulated as

$$\Delta\mu_{\alpha/\mathrm{L}}^{A*} = R_\mathrm{g}T_\mathrm{I}\left(C_\mathrm{L}^* + C_\alpha^e - C_\alpha^* - C_{\mathrm{L}\alpha}^\mathrm{e}\right),$$
$$\Delta\mu_{\alpha/\mathrm{L}}^{B*} = R_\mathrm{g}T_\mathrm{I}\ln\frac{k_\alpha}{k_{\mathrm{e}\alpha}}, \tag{29}$$

whereas for the β phase, we have

$$\Delta\mu_{\beta/\mathrm{L}}^{A*} = R_\mathrm{g}T_\mathrm{I}\ln\frac{k_\beta}{k_{\mathrm{e}\beta}},$$
$$\Delta\mu_{\beta/\mathrm{L}}^{B*} = R_\mathrm{g}T_\mathrm{I}\left(C_\beta^* + C_{\mathrm{L}\beta}^\mathrm{e} - C_\beta^* - C_\mathrm{L}^*\right). \tag{30}$$

Substituting Eqs. 24–30 into the following kinetic eutectic equations at steady-state [35]:

$$\frac{V}{V_\mathrm{DL}^\mathrm{I}} = \frac{R_\mathrm{g}T_\mathrm{I}}{C_\mathrm{L}^* - C_\alpha^*}\left(\frac{\partial\tilde{\mu}_\mathrm{L}^*}{\partial C_\mathrm{L}^*}\right)^{-1}\psi\left[1-\exp\left(\frac{\Delta\mu_{\alpha/\mathrm{L}}^{A*} - \Delta\mu_{\alpha/\mathrm{L}}^{B*}}{R_\mathrm{g}T_\mathrm{I}}\right)\right], \tag{31}$$

$$\frac{V}{V_0^{\alpha/\mathrm{L}}} = 1 - \exp\left[\frac{C_\mathrm{L}^*\Delta\mu_{\alpha/\mathrm{L}}^{B*} + \left(1-C_\mathrm{L}^*\right)\Delta\mu_{\alpha/\mathrm{L}}^{A*} - V_mK_{\alpha/\mathrm{L}}\sigma_{\alpha/\mathrm{L}}}{R_\mathrm{g}T_\mathrm{I}}\right], \tag{32}$$

$$\frac{V}{V_\mathrm{DL}^\mathrm{I}} = -\frac{R_\mathrm{g}T_\mathrm{I}}{C_\mathrm{L}^* - C_\beta^*}\left(\frac{\partial\tilde{\mu}_\mathrm{L}^*}{\partial C_\mathrm{L}^*}\right)^{-1}\psi\left[1-\exp\left(\frac{\Delta\mu_{\beta/\mathrm{L}}^{B*} - \Delta\mu_{\beta/\mathrm{L}}^{A*}}{R_\mathrm{g}T_\mathrm{I}}\right)\right], \tag{33}$$

$$\frac{V}{V_0^{\beta/\mathrm{L}}} = 1 - \exp\left[\frac{C_\mathrm{L}^*\Delta\mu_{\beta/\mathrm{L}}^{B*} + \left(1-C_\mathrm{L}^*\right)\Delta\mu_{\beta/\mathrm{L}}^{A*} - V_mK_{\beta/\mathrm{L}}\sigma_{\beta/\mathrm{L}}}{R_\mathrm{g}T_\mathrm{I}}\right]. \tag{34}$$

the non-equilibrium solute partition coefficients (k_α,k_β) and interface undercooling (ΔT_I) are given as

$$(k_i - k_{\mathrm{e}i})\psi = k_i(1-k_i)\frac{V}{V_\mathrm{DL}^\mathrm{I}} \quad (i=\alpha,\beta), \tag{35}$$

$$\Delta T_\mathrm{I} = m_{\mathrm{L}\alpha}^\mathrm{e}C_\mathrm{EL}^\mathrm{e} - m_{\mathrm{L}\alpha}C_\mathrm{L}^* - \frac{m_{\mathrm{L}\alpha}^\mathrm{e}}{1-k_{\mathrm{e}\alpha}}\frac{V}{V_0^{\alpha/\mathrm{L}}} + \frac{m_{\mathrm{L}\alpha}^\mathrm{e}}{1-k_{\mathrm{e}\alpha}}\frac{V_m\sigma_{\alpha/\mathrm{L}}}{R_\mathrm{g}T_\mathrm{I}}K_{\alpha/\mathrm{L}}, \tag{36}$$

$$\Delta T_\mathrm{I} = -m_{\mathrm{L}\beta}^\mathrm{e}\left(1-C_\mathrm{EL}^\mathrm{e}\right) + m_{\mathrm{L}\beta}\left(1-C_\mathrm{L}^*\right) + \frac{m_{\mathrm{L}\beta}^\mathrm{e}}{1-k_{\mathrm{e}\beta}}\frac{V}{V_0^{\beta/\mathrm{L}}} - \frac{m_{\mathrm{L}\beta}^\mathrm{e}}{1-k_{\mathrm{e}\beta}}\frac{V_m\sigma_{\beta/\mathrm{L}}}{R_\mathrm{g}T_\mathrm{I}}K_{\beta/\mathrm{L}}, \tag{37}$$

where

$$m_{Li} = \frac{m_{Li}^\mathrm{e}}{1-k_{\mathrm{e}i}}\left(1-k_i+\ln\frac{k_i}{k_{\mathrm{e}i}}\right) \ (i=\alpha,\beta) \tag{38}$$

is the kinetic slope of liquidus. Note that linear thermodynamics is assumed for interface migration during the derivation of Eqs. 36 and 37.

In contrast to Kurz and Trivedi [19] in which the same interface kinetic model is adopted for the α/L ($C_{E\alpha}^e < C_{EL}^e$) and β/L ($C_{E\beta}^e > C_{EL}^e$) interfaces (please see Eqs. 17–19 in Ref. [19]), the solute trapping model (Eq. 35) is the same but not the model for interface undercooling (Eqs. 36, 37). In other words, one cannot substitute directly m_{Li} for m_{Li}^e in the original TMK model [11] to incorporate non-equilibrium interface kinetics. Note that the solute trapping model is not equivalent to that of Sobolev [24], whereas, the model for interface undercooling is actually the same as the model with solute drag [17]. For the planar interface, the concentration at the TJ $C_\mathrm{L}^\wedge$ can be obtained from Eqs. 36 and 37 as

$$C_\mathrm{L}^\wedge = \frac{1}{m_{\mathrm{L}\alpha} - m_{\mathrm{L}\beta}}\left[m_{\mathrm{L}\alpha}^\mathrm{e}C_\mathrm{LE}^\mathrm{e} + m_{\mathrm{L}\beta}^\mathrm{e}\left(1-C_\mathrm{LE}^\mathrm{e}\right) - m_{\mathrm{L}\beta} - \frac{m_{\mathrm{L}\alpha}^\mathrm{e}}{1-k_{\mathrm{e}\alpha}}\frac{V}{V_0^{\alpha/\mathrm{L}}} - \frac{m_{\mathrm{L}\beta}^\mathrm{e}}{1-k_{\mathrm{e}\beta}}\frac{V}{V_0^{\beta/\mathrm{L}}}\right]. \tag{39}$$

The average interface kinetic condition for interface migration Eq. 16 can be rewritten as

$$\Delta T_\mathrm{I} = \frac{\left(m_{\mathrm{L}\alpha}^\mathrm{e}C_\mathrm{EL}^\mathrm{e} - m_{\mathrm{L}\alpha}\bar{C}_{\mathrm{L}\alpha}^*\right)\frac{\left(k_{\mathrm{e}\alpha}-1\right)V_0^{\alpha/\mathrm{L}}f_\alpha}{m_{\mathrm{L}\alpha}^\mathrm{e}} + \left[-m_{\mathrm{L}\beta}^\mathrm{e}\left(1-C_\mathrm{EL}^\mathrm{e}\right) + m_{\mathrm{L}\beta}\left(1-\bar{C}_{\mathrm{L}\beta}^*\right)\right]\frac{\left(1-k_{\mathrm{e}\beta}\right)V_0^{\beta/\mathrm{L}}f_\beta}{m_{\mathrm{L}\beta}^\mathrm{e}}}{\frac{\left(k_{\mathrm{e}\alpha}-1\right)V_0^{\alpha/\mathrm{L}}f_\alpha}{m_{\mathrm{L}\alpha}^\mathrm{e}} + \frac{\left(1-k_{\mathrm{e}\beta}\right)V_0^{\beta/\mathrm{L}}f_\beta}{m_{\mathrm{L}\beta}^\mathrm{e}}} + \frac{V}{\frac{\left(k_{\mathrm{e}\alpha}-1\right)V_0^{\alpha/\mathrm{L}}f_\alpha}{m_{\mathrm{L}\alpha}^\mathrm{e}} + \frac{\left(1-k_{\mathrm{e}\beta}\right)V_0^{\beta/\mathrm{L}}f_\beta}{m_{\mathrm{L}\beta}^\mathrm{e}}} + \frac{-\frac{V_m}{R_\mathrm{g}T_\mathrm{I}}\left(f_\alpha\sigma_{\alpha/\mathrm{L}}V_0^{\alpha/\mathrm{L}}\bar{K}_{\alpha/\mathrm{L}} + f_\beta\sigma_{\beta/\mathrm{L}}V_0^{\beta/\mathrm{L}}\bar{K}_{\beta/\mathrm{L}}\right)}{\frac{\left(k_{\mathrm{e}\alpha}-1\right)V_0^{\alpha/\mathrm{L}}f_\alpha}{m_{\mathrm{L}\alpha}^\mathrm{e}} + \frac{\left(1-k_{\mathrm{e}\beta}\right)V_0^{\beta/\mathrm{L}}f_\beta}{m_{\mathrm{L}\beta}^\mathrm{e}}} \tag{40}$$

The first, second, and third terms on the right hand side of Eq. 40 are ΔT_C, ΔT_K, and ΔT_R. One can then obtain λ, R, and ΔT for a given V by integrating Eqs. 6–9, 11, 17, 18, 21–23, 35, and 38–40.

References

1. Akamatsu S, Faivre G (2000) Traveling waves, two-phase fingers, and eutectic colonies in thin-sample directional solidification of a ternary eutectic alloy. Phys Rev E 61:3757–3770
2. Akamatsu S, Perrut M, Bottin-Rousseau S, Faivre G (2010) Spiral two-phase dendrites. Phys Rev Lett 104:056101. doi:10.1103/PhysRevLett.104.056101
3. Wei B, Herlach DM, Feuerbacher B, Sommer F (1993) Dendritic and eutectic solidification of undercooled Co-Sb alloys. Acta Metall Mater 41:1801–1809
4. Liu L, Li JF, Zhou YH (2011) Solidification interface morphology pattern in the undercooled Co–24.0 at.% Sn eutectic melt. Acta Mater 59:5558–5567
5. Mullins WW, Sekerka RF (1964) Stability of a planar interface during solidification of a dilute binary alloy. J Appl Phys 35:444–451
6. Goetzinger R, Barth M, Herlach DM (1998) Growth of lamellar eutectic dendrites in undercooled melts. J Appl Phys 84:1643–1649
7. Zryd A, Gremaud M, Kurz W (1994) Lamellar eutectics: a comparison of three models valid at high growth rates. Mater Sci Eng A 181(182):1392–1396
8. Lipton J, Kurz W, Trivedi R (1987) Rapid dendrite growth in undercooled alloys. Acta Metall 35:957–964
9. Donaghey LF, Tiller WA (1968/69) On the diffusion of solute during the eutectoid and eutectic transformations, part I. Mater Sci Eng 3:231–239
10. Li JF, Zhou YH (2005) Eutectic growth in bulk undercooled melts. Acta Mater 53:2351–2359
11. Trivedi R, Magnin P, Kurz W (1987) Theory of eutectic growth under rapid solidification conditions. Acta Metall 35:971–980
12. Liu L, Li JF, Zhou YH (2009) Solidification of undercooled eutectic alloys containing a third element. Acta Mater 57:1536–1545
13. Yang C, Gao J, Zhang YK et al (2011) New evidence for the dual origin of anomalous eutectic structures in undercooled Ni–Sn alloys: in situ observations and EBSD characterization. Acta Mater 59:3915–3926
14. Hillert M (1999) Solute drag, solute trapping and diffusional dissipation of Gibbs energy. Acta Mater 47:4481–4505
15. Wang HF, Liu F, Zhai HM, Wang K (2012) Application of the maximal entropy production principle to rapid solidification: a sharp interface model. Acta Mater 60:1444–1454
16. Aziz MJ (1982) Model for solute redistribution during rapid solidification. J Appl Phys 53:1158–1168
17. Aziz MJ, Kaplan T (1988) Continuous growth model for interface motion during alloy solidification. Acta Metall 36:2335–2347
18. Jackson KA, Hunt JD (1966) Lamellar and rod eutectic growth. Trans AIME 236:1129–1142
19. Kurz W, Trivedi R (1991) Eutectic growth under rapid solidification conditions. Metall Trans A 22:3051–3057
20. Wang N, Kalay YE, Trivedi R (2011) Eutectic-to-metallic glass transition in the Al–Sm system. Acta Mater 59:6604–6619
21. Trivedi R, Wang N (2012) Theory of rod eutectic growth under far-from-equilibrium conditions: nanoscale spacing and transition to glass. Acta Mater 60:3140–3150
22. Herlach DM (1994) Non-equilibrium solidification of undercooled metallic melts. Mater Sci Eng Rep R 12:177–272
23. Jou D, Casas-Vázquez J, Lebon G (2010) Extended irreversible thermodynamics. Springer, Berlin
24. Sobolev SL (1995) Local-nonequilibrium model for rapid solidification of undercooled melts. Phys Lett A 199:383–386
25. Galenko P (2007) Solute trapping and diffusionless solidification in a binary system. Phys Rev E 76:031606. doi:10.1103/PhysRevE.76.031606
26. Galenko PK, Danilov DA (1997) Local nonequilibrium effect on rapid dendritic growth in a binary alloy melt. Phys Lett A 235:271–280
27. Galenko PK, Danilov DA (1999) Model for free dendritic alloy growth under interfacial and bulk phase nonequilibrium conditions. J Cryst Growth 197:992–1002
28. Yang Y, Humadi H, Buta D et al (2011) Atomistic simulations of nonequilibrium crystal-growth kinetics from alloy melts. Phys Rev Lett 107:025505. doi:10.1103/PhysRevLett.107.025505
29. Galenko PK, Herlach DM (2006) Diffusionless crystal growth in rapidly solidifying eutectic systems. Phys Rev Lett 96:150602. doi:10.1103/PhysRevLett.96.150602
30. Akamatsu S, Plapp M, Faivre G, Karma A (2002) Pattern stability and trijunction motion in eutectic solidification. Phys Rev E 66:030501. doi:10.1103/PhysRevE.66.030501
31. Akamatsu S, Plapp M, Faivre G, Karma A (2004) Overstability of lamellar eutectic growth below the minimum-undercooling spacing. Metal Mater Trans A 35A:1815–1828
32. Wang HF, Liu F, Herlach DM (2014) On the solution of solute diffusion during eutectic growth. J Cryst Growth 389:68–73
33. Kurz W, Fisher DJ (1998) Fundamentals of solidification, 4th edn. Trans Tech, Switzerland
34. Dantzig JA, Rappaz M (2009) Solidification. EPFL Press, Switzerland
35. Wang HF, Liu F, Herlach DM (2015) Kinetics of triple-junctions in eutectic solidification: a sharp interface model. J Mater Sci 50:176–188. doi:10.1007/s10853-014-8577-5
36. Kuang WW, Karrasch C, Wang HF, Liu F, Herlach DM (2015) Eutectic dendrite growth in undercooled Fe83B17 alloy: experiments and modeling. Scr Mater 105:34–37
37. Boettinger WJ, Coriell SR, Trivedi R (1988) In: Mehrabian R, Parrish PA (eds) Rapid solidification processing: principles and technologies IV. Claitor's, Baton Rouge, LA
38. Wang K, Wang HF, Liu F, Zhai HM (2013) Modeling rapid solidification of multi-component concentrated alloys. Acta Mater 61:1359–1372
39. Wang HF, Liu F, Yang W et al (2008) An extended morphological stability model for a planar interface incorporating the effect of nonlinear liquidus and solidus. Acta Mater 56:2592–2601
40. Wang HF, Liu F, Wang K, Zhai HM (2011) Oscillatory morphological stability for rapid directional solidification: effect of non-linear liquidus and solidus. Acta Mater 59:5859–5867
41. Wang K, Wang HF, Liu F, Zhai HM (2014) Morphological stability analysis for planar interface during rapidly directional solidification of concentrated multi-component. Acta Mater 67:220–231
42. Wang HF, Liu F, Chen Z, Yang GC, Zhou YH (2007) Analysis of non-equilibrium dendrite growth in a bulk undercooled alloy melt: model and application. Acta Mater 55:497–506
43. Wang HF, Liu F, Chen Z, Yang W, Yang GC, Zhou YH (2007) Effect of non-linear liquidus and solidus in undercooled dendrite growth: a comparative study in Ni–0.7 at.% B and Ni–1 at.% Zr. Scripta Mater 57:413–416
44. Wang K, Wang HF, Liu F, Zhai HM (2013) Modeling dendrite growth in undercooled concentrated multi-component alloys. Acta Mater 61:4254–4265

45. Galenko PK, Reutzel S, Herlach DM et al (2007) Modelling of dendritic solidification in undercooled dilute Ni–Zr melts. Acta Mater 55:6834–6842
46. Galenko PK, Reutzel S, Herlach DM et al (2009) Dendritic solidification in undercooled Ni–Zr–Al melts: experiments and modeling. Acta Mater 57:6166–6175
47. Clopet CR, Cochrane RF, Mullis AM (2013) The origin of anomalous eutectic structures in undercooled Ag–Cu alloy. Acta Mater 61:6894–6902
48. Subramantan PR, Perepzko JH (1993) The Ag-Cu (Silver-Copper) system. J Phase Equilib 14:62–75
49. Wang H, Herlach DM, Liu RP (2014) Dendrite growth in Cu50Zr50 glass-forming melts, thermodynamics vs. kinetics. Europhys Lett 105:36001. doi:10.1209/0295-5075/105/36001
50. Walder S, Ryder PL (1993) Nonequilibrium solidification in undercooled melts of the alloy Ag39.9 at.% Cu. J Appl Phys 73:1965–1970
51. Walder S, Ryder PL (1993) Critical solidification behavior of undercooled Ag-Cu alloys. J Appl Phys 74:6100–6106
52. Zhao S, Li JF, Liu L, Zhou YH (2009) Cellular growth of lamellar eutectics in undercooled Ag–Cu alloy. Mater Charact 60:519–524
53. Zhao S, Li JF, Liu L, Zhou YH (2009) Solidification of undercooled Ag–Cu eutectic alloy with the Sb addition. J Alloys Compd 478:252–256